



**HAL**  
open science

## Near-infrared emitting fluorescent homobimetallic gold(I) complexes displaying promising in vitro and in vivo therapeutic properties

Robin Lescure, Malorie Privat, Jacques Pliquett, Aurélie Massot, Océane Baffroy, Benoit Busser, Pierre-Simon Bellaye, Bertrand Collin, Franck Denat, Ali Bettaïeb, et al.

### ► To cite this version:

Robin Lescure, Malorie Privat, Jacques Pliquett, Aurélie Massot, Océane Baffroy, et al.. Near-infrared emitting fluorescent homobimetallic gold(I) complexes displaying promising in vitro and in vivo therapeutic properties. *European Journal of Medicinal Chemistry*, 2021, 220 (4), pp.113483. 10.1016/j.ejmech.2021.113483 . hal-03436249

**HAL Id: hal-03436249**

**<https://hal.science/hal-03436249>**

Submitted on 9 May 2023

**HAL** is a multi-disciplinary open access archive for the deposit and dissemination of scientific research documents, whether they are published or not. The documents may come from teaching and research institutions in France or abroad, or from public or private research centers.

L'archive ouverte pluridisciplinaire **HAL**, est destinée au dépôt et à la diffusion de documents scientifiques de niveau recherche, publiés ou non, émanant des établissements d'enseignement et de recherche français ou étrangers, des laboratoires publics ou privés.



Distributed under a Creative Commons Attribution - NonCommercial 4.0 International License

## Near-infrared emitting fluorescent homobimetallic gold(I) complexes displaying promising *in vitro* and *in vivo* therapeutic properties

Robin Lescure,<sup>a‡</sup> Malorie Privat,<sup>a,b‡</sup> Jacques Pliquett,<sup>a,b</sup> Aurélie Massot,<sup>b</sup> Océane Baffroy,<sup>a</sup> Benoit Busser,<sup>c,d</sup> Pierre-Simon Bellaye,<sup>e</sup> Bertrand Collin,<sup>a,e</sup> Franck Denat,<sup>a</sup> Ali Bettaïeb,<sup>b</sup> Lucie Sancey,<sup>c</sup> Catherine Paul,<sup>b\*</sup> Christine Goze,<sup>a\*</sup> Ewen Bodio<sup>a\*</sup>

<sup>a</sup> ICMUB UMR6302, CNRS, Univ. Bourgogne Franche-Comté, F-21000 Dijon, France

E-mail: [christine.goze@u-bourgogne.fr](mailto:christine.goze@u-bourgogne.fr); [ewen.bodio@u-bourgogne.fr](mailto:ewen.bodio@u-bourgogne.fr)

Tel: +33(0)3 803 96 076; +33(0)3 803 937 73

<sup>b</sup> Laboratoire d'Immunologie et Immunothérapie des Cancers (LIIC, EA7269), EPHE, PSL Research University, F-75000, Paris, France, Université de Bourgogne Franche Comté, F-21000, Dijon, France

E-mail: [catherine.paul@u-bourgogne.fr](mailto:catherine.paul@u-bourgogne.fr)

Tel: +33(0)3 803 93 351

<sup>c</sup> Institute for Advanced Biosciences, Centre de Recherche UGA / INSERM U1209 / CNRS UMR5309, F-38700 La Tronche, France

<sup>d</sup> Grenoble Alpes University Hospital, F-38042 Grenoble, France

<sup>e</sup> Centre Georges François Leclerc, Service de médecine nucléaire, plateforme d'imagerie et de radiothérapie préclinique, 1 rue Professeur Marion, BP77980, 21079 Dijon Cedex, France

‡ These authors contributed equally

**Abstract:** Three near-infrared (NIR-I) optical theranostic systems were synthesized, characterized and studied *in vitro* and *in vivo*. These original homo-bimetallic gold(I)-based aza-BODIPY complexes proved to be trackable through near-infrared optical imaging in cells and in mice. They display anti-proliferative properties in micromolar range against human and murine cancer cell lines (4T1, MDA-MB-231, CT26, and SW480). Moreover, the injection of the most promising theranostic agent in CT26 tumor-bearing BALB/c mice induced a significant anti-cancer activity.

### INTRODUCTION

Developing new therapeutic agents is a complex task. For a long time, many researchers have focused their research on the development of therapeutic agents with the highest cytotoxicity *in vitro* without worrying about pharmacokinetics or pharmacodynamics, which has often led to failure, when the compounds were tested *in vivo*. Indeed, the ideal compound must not only be effective when it is in contact with its target, it must also be able to reach it without being degraded, accumulate at the right place in sufficient quantity, be safe for healthy tissues... The problem is that the different criteria to be improved to obtain an ideal compound are related to each other and fine tuning one by modifying the molecule can be detrimental to another one (e.g. increasing the stability of a product can decrease its therapeutic effect). It is therefore preferable to control as many parameters as possible to maximize the success of optimization of the therapeutic agent. In particular, knowing where the compound accumulates, in what quantity, by which routes it is eliminated, is crucial to rationalize the optimization. There are many techniques that can be used to do this follow-up, however, most of them are invasive and require numerous samples or animals. One more and more popular solution is the use of molecular imaging. Indeed, by grafting an imaging probe onto a therapeutic agent, it can be followed in real time and non-invasively and, thus, it is possible to collect numerous valuable information on the resulting trackable therapeutic agent thus formed (often also called theranostics).<sup>[1–6]</sup>

Like us, different research groups have opted for optical fluorescence imaging.<sup>[1,4,7–18]</sup> For example, BODIPY fluorophores were used many times *in vitro* to track therapeutically relevant metals

such as Au, Cu, Ir, Os, Pt, Rh, Ru, Ti... Some examples are given on Figure 1 (the subject was reviewed recently[7]).[4,6,7,19] The choice of optical imaging for such a tracking could be explained by the fact that it is a versatile, sensitive, non-invasive, and non-ionizing technique, involving inexpensive equipment compared to most other imaging modalities and limited constraints. Its major drawback is its low penetrability of biological tissues, which means that today the monitoring of theranostic agents by optical imaging is mainly limited to studies on cells. The objective of the present study is to demonstrate that the use of recent and innovative fluorophores – such as aza-BODIPYs – allows such monitoring *in vivo* by optical imaging, while maintaining good anti-tumor activity of the therapeutic part.

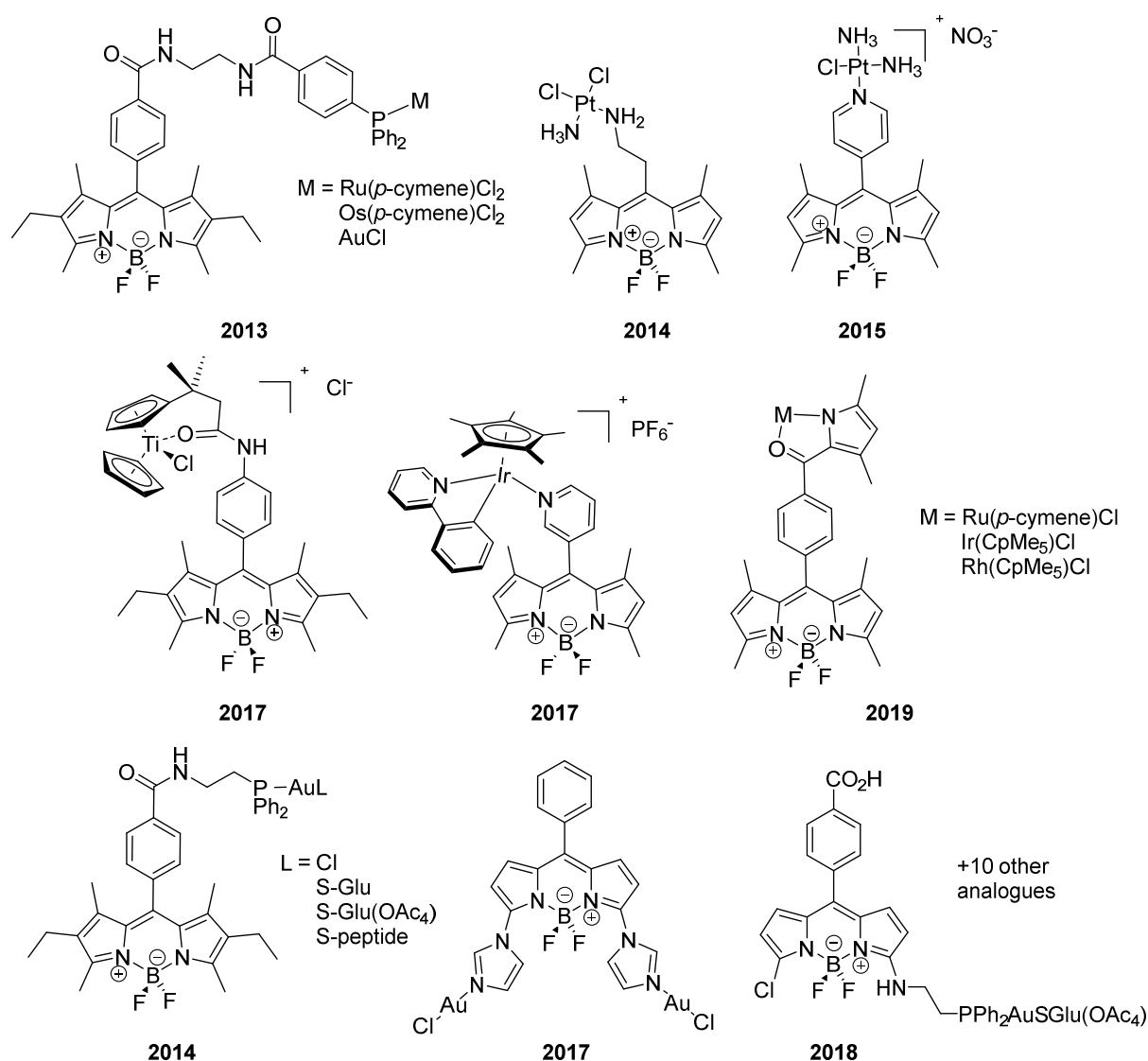


**Figure 1:** Examples of metal-based BODIPY trackable therapeutics associated with their year of publication.

Our choice fell on a gold complex for the therapeutic part because unlike most of other metal ions, gold(I) does not quench fluorescence, and because of its therapeutic properties. [4,10,13,17,20] Indeed, gold complexes exhibit many biological properties: they can act as antibacterial, antiviral, antiparasitic agents, and they increasingly appear as a promising alternative to platinum complexes to fight cancer.[21–27] In particular, auranofin – clinically used for rheumatoid arthritis – has been repurposed recently as an anticancer drug.[28–32] Several clinical trials are testing its efficacy against recurrent epithelial ovarian, primary peritoneal, or fallopian tube cancer [NCT01747798, NCT03456700], lung cancer [NCT01737502], but also leukemia [NCT01419691].[31] Numerous

targets have been reported for explaining the mechanism of action of gold complexes.[26] Concerning gold(I) complexes except topoisomerase,[21] most of the suggested targets of gold(I) complexes are enzymes, which are not localized in cell nuclei. This point is key because we are working on BODIPY and aza-BODIPY-based fluorescent platforms, which accumulate in the cell cytoplasm.[33–35] Among these enzymes, we can cite glutathione reductase, cysteine protease, and the most commonly studied are thioredoxin reductases (TrxRs).[20,36,37] All these enzymes contain thiols and/or selenol. The fact that gold complexes would target these enzymes is attributed to the strong binding affinity of gold ions for thiols.

For this study, we decided to focus on aza-BODIPY platforms because we wanted to track gold complexes both *in vitro* and *in vivo* and aza-BODIPY dyes emit in the near infrared (NIR, 700 – 900 nm for NIR I), an area of the electromagnetic spectrum where biological tissues are more transparent, scattering phenomenon is reduced, and the light toxicity is limited. Aza-BODIPY fluorophores are chemically and photochemically stable, exhibit good quantum yield and, unlike many fluorophores emitting in NIR, are easy to functionalize. Their main drawback, like most organic fluorophores, is their low solubility in water. However, we recently showed that the substitution of the fluorine atoms present on the boron atom of the aza-BODIPY core by ammonium arms made it possible to significantly improve the water-solubility of this type of fluorophores and to limit aggregation phenomena.[35,38,39] In addition, it is possible to use advantageously these arms to introduce different groups of interest,[35,39,38,40] such as the two phosphines-gold, we decided to introduce as therapeutic moieties (Figure 2).

Aza-BODIPYs have been used as trackable therapeutic agents for photodynamic therapy (PDT)[41,42] or to monitor boron clusters for boron neutron capture therapy (BNCT).[38,39] However, the previous study reporting an assay for tracking a cytotoxic metal complex – an analogue of carboplatin – led to the loss of anti-proliferative activity.[43] The present study will describe not only the synthesis and characterization of three innovative aza-BODIPY-based gold(I) complexes, but also the evaluation of their biological properties as well as their efficiency for *in vitro* imaging. Moreover, the *in vivo* anti-cancer activity of the most promising complex and its ability to be tracked *in vivo* by optical imaging was also investigated.

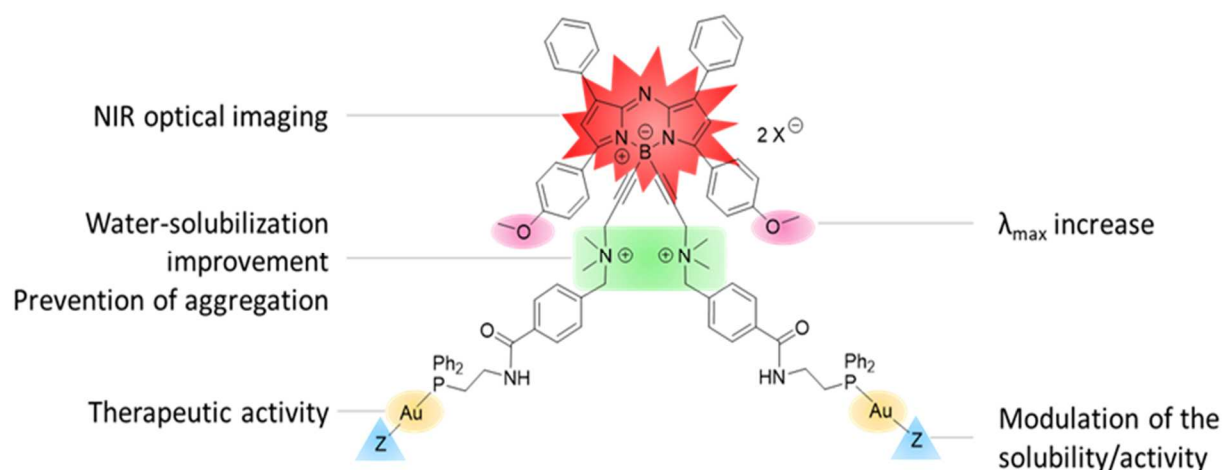


**Figure 2:** Targeted theranostics and rationale for the chosen functionalizations.

## RESULTS AND DISCUSSION

### Synthesis of gold-based complexes and photophysical characterization

The first step is the synthesis of the bis-acid platform **Wazaby7** (Scheme 1). This platform was designed for *in vivo* applications due to its good water solubility and its excitation and emission in NIR (the presence of the methoxy group in para position of the aromatic ring allows a bathochromic shift in comparison to phenyl). **Wazaby7** was synthesized in two steps, starting from the corresponding difluoro-aza-BODIPY **1**, following the method we previously reported[44]: substitution of the fluorine atoms of the boron center using the Grignard reagent of *N,N*-dimethylpropargylamine, leading to compound **2**, followed by the quaternization of the amino groups. It is worth noting that **Wazaby7** platform can be synthesized in less than five days in gram-scale. Gold(I) complexes were then introduced *via* peptidic coupling reaction with more than 80% yield to give **azaBODI-Au-1** (Scheme 1). It should be noted that the chloride counter-anions present in **Wazaby7** (due to the treatment with HCl at the end of the reaction), are partially replaced by  $\text{PF}_6^-$  anions coming from the HBTU (Hexafluorophosphate Benzotriazole Tetramethyl Uronium) coupling agent. In order to have only chloride counter-anions, we subjected **azaBODI-Au-1** to an anion exchange on resin that can be checked by ionic chromatography and  $^{31}\text{P}$ -NMR (Figure 3).

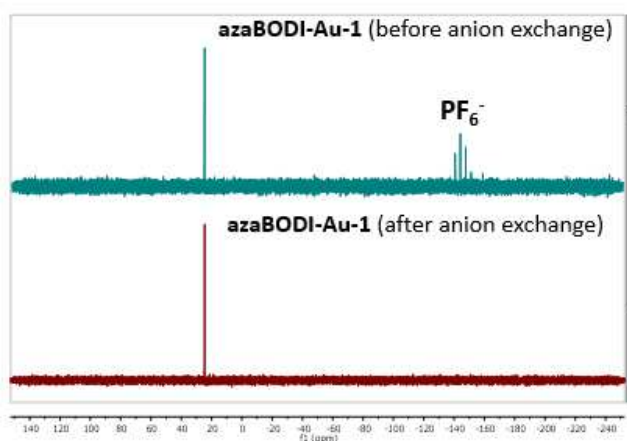


**Figure 3:**  $^{31}\text{P}$ -NMR of **azaBODI-Au-1** before (up) and after (bottom) anion exchange

This first trackable therapeutic agent can be easily modified by reacting **azaBODI-Au-1** with a thiol in the presence of a base. The reaction can be easily monitored by  $^{31}\text{P}$ -NMR (Figure 4). Indeed, the substitution of the chlorido ligand by the sulfur derivative results in a downfield of the signal in  $^{31}\text{P}$ -NMR, as well as a strong widening of the latter, as usually observed for such a ligand exchange.[16,45,46]

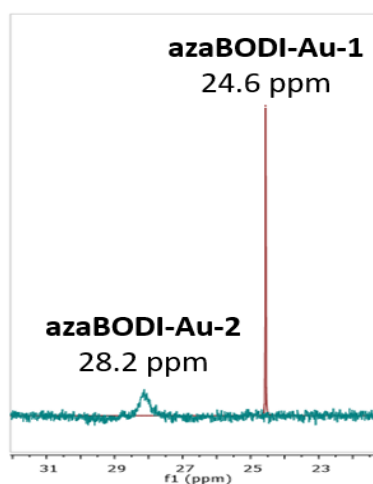
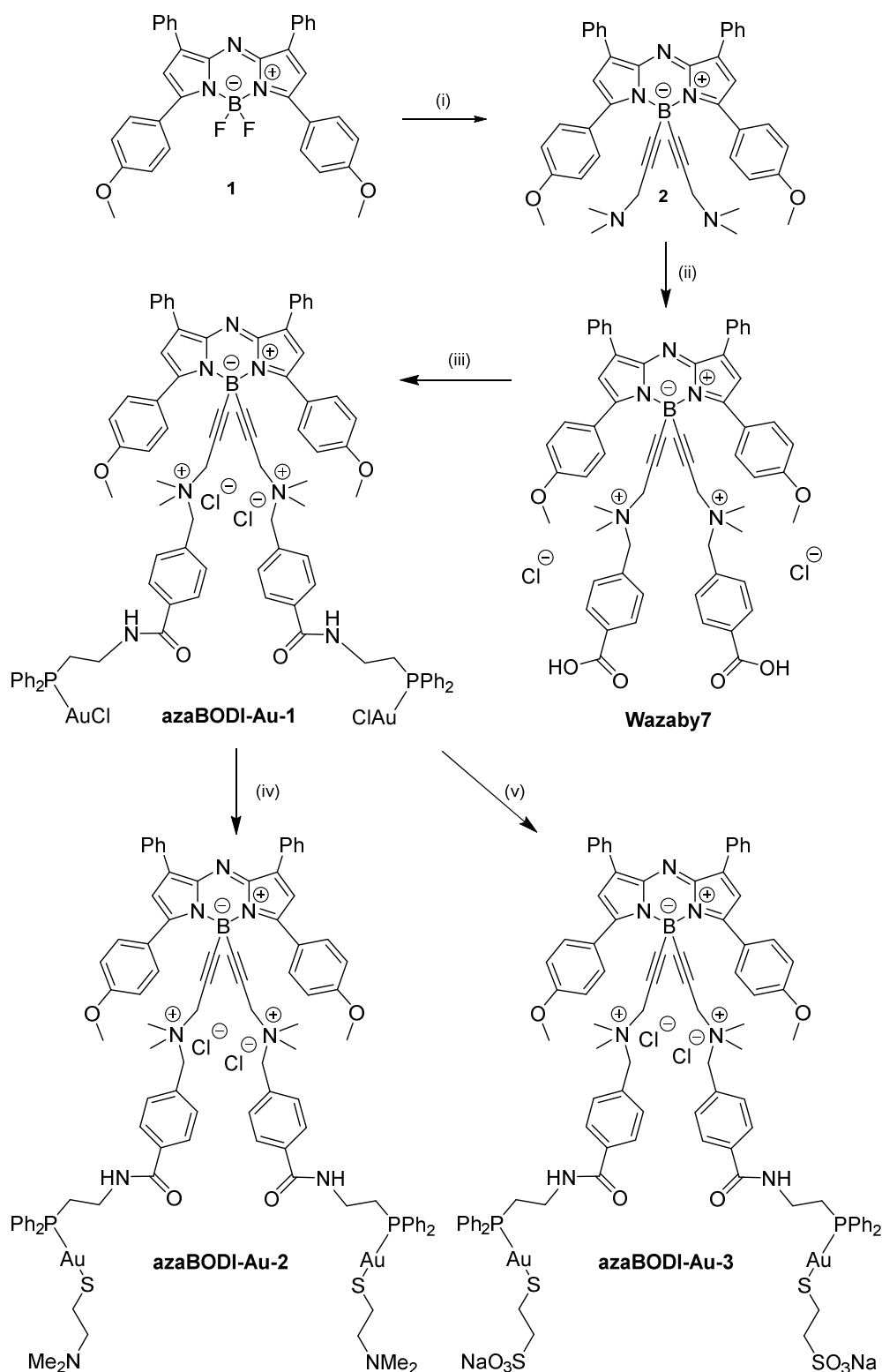


**Figure 4:**  $^{31}\text{P}$ -NMR of **azaBODI-Au-1** (red) and **azaBODI-Au-2** (blue)



**Scheme 1:** Syntheses of the three theranostics starting from the water-soluble platform corresponding “BF<sub>2</sub>” Aza-BODIPY 2 ((i) *N,N*-dimethylpropargylamine, EtMgBr, THF, 1.5 h, reflux; (ii) 4-(bromomethyl)benzoic acid, NaHCO<sub>3</sub>, THF/H<sub>2</sub>O, 5 h, r.t.; (iii) HBTU, DIPEA, [Au(Cl)P(Ph)<sub>2</sub>CH<sub>2</sub>CH<sub>2</sub>NH<sub>2</sub>], DMF, 4 h, r.t.; (iv) [HSCH<sub>2</sub>CH<sub>2</sub>NMe<sub>2</sub>·HCl], DIPEA, DCM, 20 h, 0 °C→r.t.; (v) HSCH<sub>2</sub>CH<sub>2</sub>SO<sub>3</sub>Na, NaOH, acetone, 3 h, 0 °C→12 °C).

We chose two different thiols: one bearing a dimethylamino group and another one bearing a sulfonate. Our objective was to study the impact of the overall charge of the trackable therapeutic

agent (or theranostic) on its biological properties. Indeed, it has been shown that it can have an impact on the cellular uptake,[47] the mode of transport in the cells[48], etc. At physiological pH, **azaBODI-Au-1** possesses two positive charges (two ammonium arms), **azaBODI-Au-2** can be charged 4+ (two ammonium arms and protonation of the two NMe<sub>2</sub> groups brought by the thiolato ligand), and **azaBODI-Au-3** is neutral (two ammonium arms and two negative charges brought by the two sulfonates). Another interest of exchanging the chlorido ligand of gold center by a thiolate is the fact that the resulting complexes will be more thermodynamically stable.[49] It will be interesting to investigate if this higher stability will improve the activity of the complexes or if it will be detrimental. The three gold(I)-aza-BODIPY complexes underwent ion exchange on resin to obtain chlorides as counter-anions.

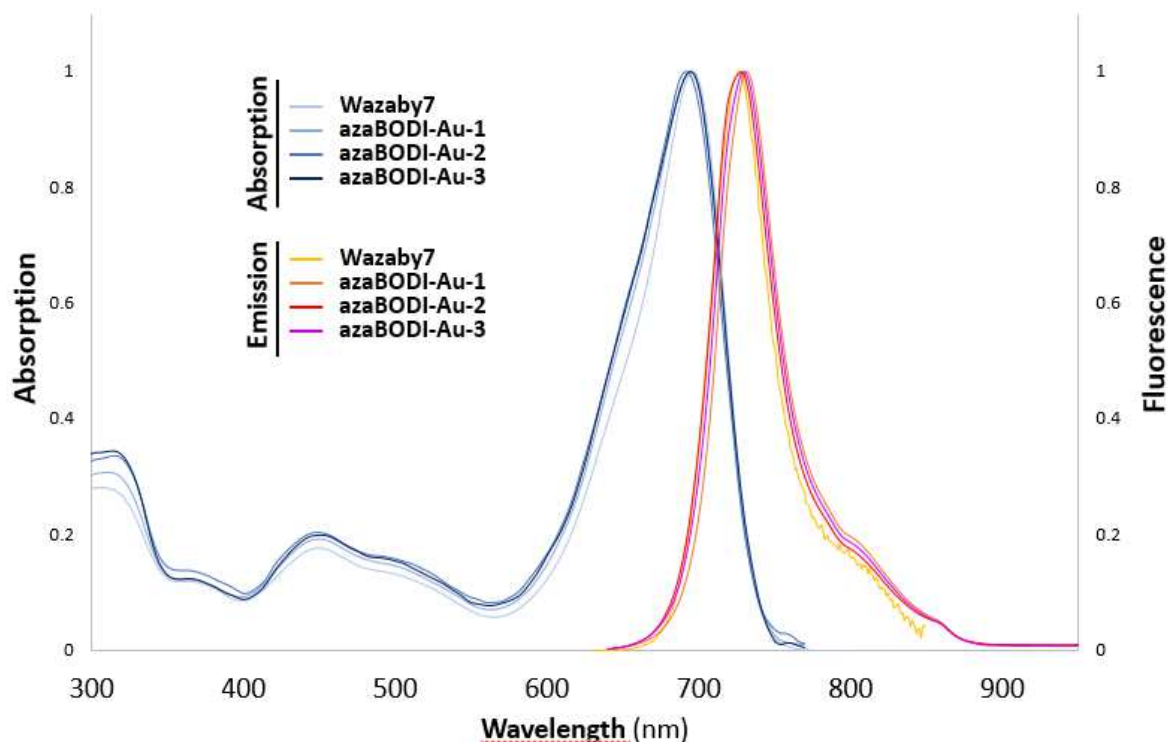


**Figure 5:** Absorption and emission spectra of **Wazaby7**, **azaBODI-Au-1**, **azaBODI-Au-2**, and **azaBODI-Au-3** in DMSO at 25 °C (absorption and emission are normalized).

The photophysical properties of the three novel homo-bimetallic complexes **azaBODI-Au-1**, **azaBODI-Au-2**, and **azaBODI-Au-3**, as well as the corresponding bis-acid aza-BODIPY – **Wazaby7** – were investigated (Table 1). As expected, the different aza-BODIPY derivatives display a maximal absorption wavelength around 694 nm, corresponding to the S<sub>0</sub>-S<sub>1</sub> transition band and with a high coefficient absorption (between 60,000 and 70,000 M<sup>-1</sup>.cm<sup>-1</sup>), and the second S<sub>0</sub>-S<sub>2</sub> band appearing at around 450 nm for the three systems. All the different complexes possess a maximal fluorescence emission wavelength around 730 nm with relatively high quantum yields (Table 1). Moreover, we confirm the strong photobleaching resistance of our aza-BODIPY (under the same irradiation conditions, the brightness of **azaBODI-Au-1** decreases of around 30% vs around 80% for ICG). Interestingly, the introduction of the two gold(I)-complexes as well as the ligand exchanges do not significantly affect the photophysical properties of the aza-BODIPYs, as we could observe previously.[4,50] The absorption and emission spectra are almost superimposable and the brightness is similar for all the compounds (Figure 5). The excitation spectra also match the absorption spectra for all the compounds, confirming the presence of one S<sub>1</sub>-S<sub>0</sub> single emitting state.

**Table 1:** Main photophysical data of **Wazaby7**, **azaBODI-Au-1**, **azaBODI-Au-2**, and **azaBODI-Au-3** in DMSO at 298 K.

Compound	$\lambda_{\max, \text{abs}}$ (nm)	$\lambda_{\max, \text{em}}$ (nm)	$\epsilon_{\lambda, \max}$ ( $\text{M}^{-1} \cdot \text{cm}^{-1}$ )	$\Phi^*$ (%)	Br ( $\text{M}^{-1} \cdot \text{cm}^{-1}$ )
<b>Wazaby7</b>	694	727	60,000	32	19,200
<b>azaBODI-Au-1</b>	695	732	70,700	27	19,090
<b>azaBODI-Au-2</b>	693	728	68,100	29	19,750
<b>azaBODI-Au-3</b>	695	730	64,000	25	16,000

\* reference: aza-BODIPY **1**  $\phi_F = 36\%$  in chloroform, 298 K,  $\lambda_{\text{exc}} = 620 \text{ nm}$ [51]

### *In vitro* investigations

The anti-proliferative properties of the three gold(I)-based aza-BODIPY were investigated in murine and human breast (4T1 and MDA-MB-231, respectively) or colon (CT26 and SW480, respectively) cancer cell lines, and on normal cell line (HMEC, human mammary epithelial cells) (Table 2). The aza-BODIPYs complexes were then compared with auranofin as a benchmark gold-based therapeutic (Table 2). **AzaBODI-Au-1**, **azaBODI-Au-2**, and **azaBODI-Au-3** exhibit strong anti-proliferative activities. Indeed, even if auranofin displays slightly lower  $\text{IC}_{50}$  values, values below  $10 \mu\text{M}$  are rare for metal complexes tethered to a fluorophore. In our previous studies, the gold(I)-based theranostics, whether the fluorophore was a coumarin, a BODIPY or another organic fluorophore, exhibited anti-proliferative activities of the order of 30 to  $80 \mu\text{M}$ . One hypothesis could be that the Wazaby platform carries two gold complexes, but this has to be confirmed as some studies show that the correlation is not obvious.[4] We can also notice that **AzaBODI-Au-1** and **azaBODI-Au-3** gave the same results, whereas **azaBODI-Au-2** showed more limited activity on the 4T1, CT26, and SW480 cells. As a control, the anti-proliferative properties of compound **1** and **Wazaby7** were investigated onto the four cancer cell lines and display  $\text{IC}_{50} > 100 \mu\text{M}$ , which highlights that the toxicity does not come from azaBODIPY backbone. It is also worth noting, that the three theranostics display comparable  $\text{IC}_{50}$  on healthy cell line and on cancer ones (healthy cells are known to be very sensitive), whereas auranofin is so toxic on HMEC that its  $\text{IC}_{50}$  is lower than  $0.5 \mu\text{M}$ .

To go deeper into the mechanism of action of the different compounds, we measured the quantity of gold in the cells by ICP-MS after 4 hours of incubation of  $5 \mu\text{M}$  of gold complexes (Table 3). It clearly appears that the complexes with chlorido ligands - **azaBODI-Au-1** and auranofin - accumulate significantly less than those with thiolato ligands. If we keep in mind that there are two gold equivalents per **azaBODI-Au-1** and only one for auranofin, we can consider that they accumulate in a similar way. In contrast, **azaBODI-Au-3** accumulates significantly more than **azaBODI-Au-2**. It may be an impact of the global charge of the molecule, because, as indicated before and without considering the counter ions, **azaBODI-Au-3** is globally neutral while **azaBODI-Au-2** is charged 4+. Based on these results, it appears that the anti-proliferative properties of the compounds cannot be directly related to their ability to accumulate in cells. On the other hand, it seems that the "Au-Cl" complex is more active than the "Au-S" ones. Indeed, **azaBODI-Au-1** accumulates 1.6 to 4.5 times less than **azaBODI-Au-3**, while exhibiting the same activities.

**Table 2:**  $\text{IC}_{50}$  values ( $\mu\text{M}$ ), determined by MTS assay at 48 h, of **azaBODI-Au-1**, **azaBODI-Au-2**, **azaBODI-Au-3**, and auranofin on 4T1, MDA-MB-231, CT26, SW480, and HMEC cell lines.

Compounds	$\text{IC}_{50} \pm \text{SEM}$ ( $\mu\text{M}$ )				
	4T1	MDA-MB-231	CT26	SW480	HMEC
<b>azaBODI-Au-1</b>	$4.3 \pm 0.5$	$9.7 \pm 0.7$	$4.1 \pm 0.2$	$4.2 \pm 0.5$	$3.4 \pm 0.9$
<b>azaBODI-Au-2</b>	$9.9 \pm 0.6$	$10.2 \pm 0.2$	$10.1 \pm 0.5$	$10.2 \pm 0.6$	$5.6 \pm 0.1$
<b>azaBODI-Au-3</b>	$4.8 \pm 0.4$	$9.2 \pm 0.6$	$4.5 \pm 0.6$	$4.3 \pm 0.6$	$5.0 \pm 0.1$
auranofin	$3.4 \pm 0.9$	$2.1 \pm 1.0$	$2.5 \pm 0.5$	$2.1 \pm 0.7$	$< 0.5$

**Table 3:** Cellular uptake of **azaBODI-Au-1**, **azaBODI-Au-2**, **azaBODI-Au-3**, and auranofin in 4T1, MDA-MB-231, and CT26 cells treated or not (control) with 5  $\mu\text{M}$  of metal complexes for 4 h at 37  $^{\circ}\text{C}$  analyzed by ICP-MS.

Compounds	Gold uptake (mg Au / g protein)		
	4T1	MDA-MB-231	CT26
Untreated cells	< 0.5	< 0.5	< 0.5
<b>azaBODI-Au-1</b>	15.3	7.2	13.3
<b>azaBODI-Au-2</b>	24.1	11.9	15.9
<b>azaBODI-Au-3</b>	29.6	32.6	21.8
auranofin	10.5	3.0	3.7

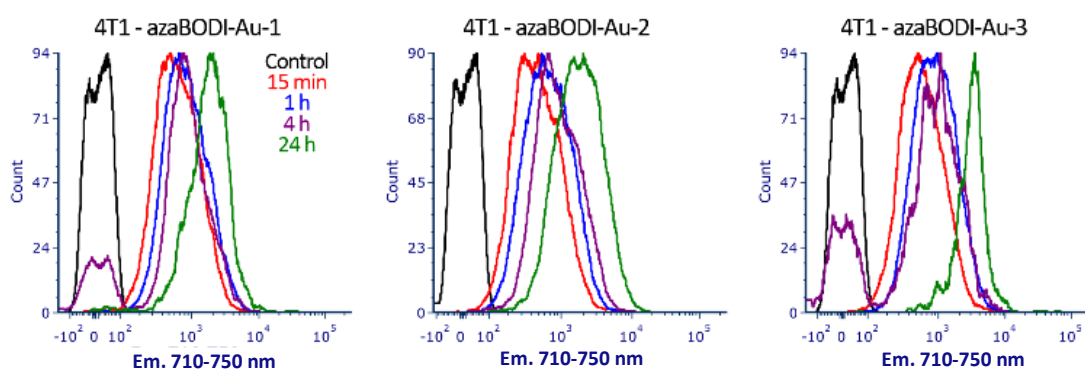


**Figure 6:** Histograms of 4T1 cells incubated with **azaBODI-Au-1**, **azaBODI-Au-2**, and **azaBODI-Au-3** at 5  $\mu\text{M}$  from flow cytometry measurements. The fluorescence signal was collected using a band pass filter 730/40 nm.

As the compounds are fluorescent, it was also possible to determine their accumulation in cells by FACS analysis. This technique is less precise, but it is faster and less expensive than the ICP-MS assays. Thus, the cell uptake was confirmed by FACS analysis for **azaBODI-Au-1**, **azaBODI-Au-2**, and **azaBODI-Au-3**, but not for auranofin (Figure 6). The three compounds efficiently accumulated in a time-dependent manner in the cells (Figure 6, Figure S18, and Figure S19). Indeed, the fluorescence intensity is already high at 15 min and gradually increases up to 24 hours.

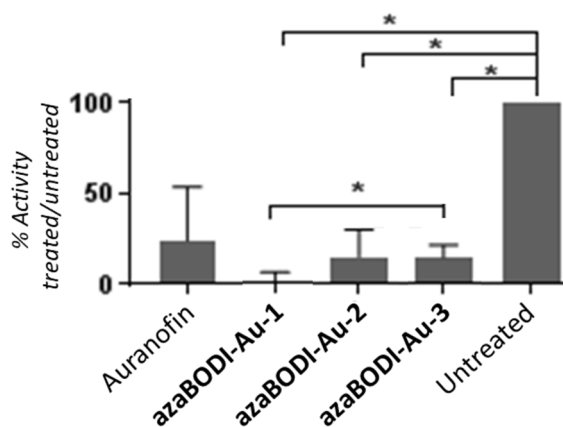


**Figure 7:** Normalized activity of TrxRs from CT26 cells treated with 5  $\mu\text{M}$  of the **azaBODI-Au-1**, **azaBODI-Au-2**, **azaBODI-Au-3**, and auranofin during 24 h (n = 4). Results are expressed as mean %  $\pm$  SEM, Student t-test: \*p  $\leq$  0.05.

As stated before, the capacity of complexes to accumulate in cells is not sufficient to explain their anti-proliferative properties. We therefore decided to study their ability to inhibit the activity of thioredoxin reductases (TrxRs), a potential target of gold(I) complexes. The inhibition of these enzymes, upregulated in certain cancers and regulating oxidative stress, results in cell apoptosis. From a mechanistic point of view, the selenocysteine of these enzymes would replace the ligand "X" of the gold complex (chlorido or thiolato), which would induce the inhibition of TrxRs. We then evaluated the activity of the TrxRs after incubation of the CT26 cells in the presence of the gold complexes. At 5  $\mu$ M, **azaBODI-Au-1**, **azaBODI-Au-2**, **azaBODI-Au-3**, and auranofin strongly inhibits TrxRs (Figure 7). In particular, the activity of TrxRs is almost undetectable for **azaBODI-Au-1**, whereas it is reduced by a factor of four to ten for the other complexes. Taking into account that **azaBODI-Au-1** accumulates less in cells than **azaBODI-Au-2** and **azaBODI-Au-3**, it is clear that its ability to inhibit TrxRs is much greater. This could partly explain why its relatively low accumulation is not correlated with a lower anti-proliferative activity. Such a difference in terms of inhibition of TrxRs can be explained, as mentioned above, by a difference in reactivity between the "Au-Cl" and "Au-S" bonds with respect to the enzyme. It can also be mentioned the accessibility of the gold center, which is easier in the case of **azaBODI-Au-1** because the chlorido ligand is less bulky than those of **azaBODI-Au-2** and **azaBODI-Au-3**. In addition, the **azaBODI-Au-2** and **azaBODI-Au-3** "X" ligands are either positively or negatively charged, which may hinder the approach of the enzyme. It should also be noted that even if **azaBODI-Au-1** inhibits significantly more TrxRs than **azaBODI-Au-3** into CT26 cell line, they display similar anti-proliferative properties, thus, it is not possible to make a strict correlation between inhibition of TrxRs and anti-proliferative properties.

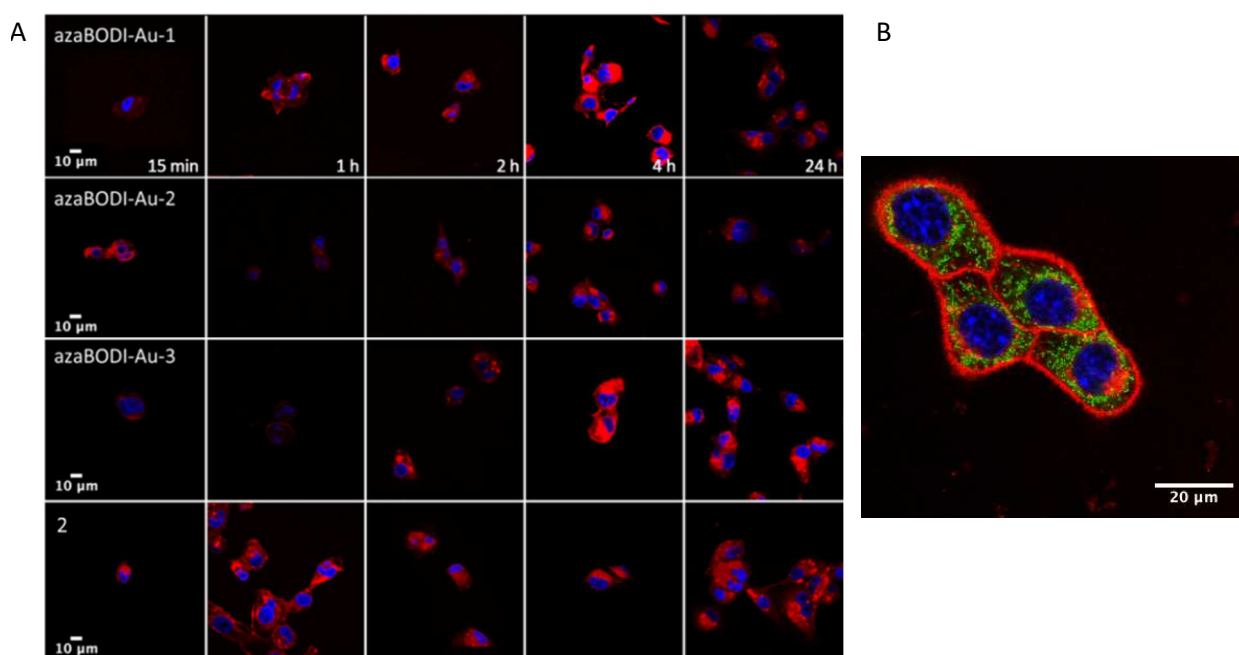


**Figure 8:** A- Confocal microscopy imaging (merge) of MDA-MB-231 cells labelled with compound **2**, **azaBODI-Au-1**, **azaBODI-Au-2**, and **azaBODI-Au-3**. Cells were incubated with the aza-BODIPY derivative (red) at 5  $\mu$ M for 15 min, 1 h, 2 h, 4 h, and 24 h at 37  $^{\circ}$ C. The nuclei are counterstained with Hoechst 33342 (blue, fluorescent DNA dye). B- Confocal microscopy imaging (merged) of 4T1 cells labelled with **azaBODI-Au-1**. Mitochondria were labeled using Mito-tracker green (Life Technology), nuclei are counterstained with Hoechst 33342 (blue, fluorescent DNA dye), and **azaBODI-Au-Cl** (red) was incubated at 5  $\mu$ M for 45 minutes.

In order to complete this *in vitro* study, we took advantage of our compounds being trackable by optical imaging to visualize their localization in cells at different times. The experiments were

conducted on human MDA-MB-231 cells (Figure 8A, Figure S15) and mouse 4T1 cells (Figure S16). The confocal imaging demonstrated a fast and efficient cell internalization of the three theranostics as well as aza-BODIPY 2 (Figure 8A, Figure S15, and figure S16). They mainly localized inside small cytoplasmic vesicles and close to the nucleus, at longer time they seem to accumulate in Golgi apparatus. One should note the absence of gold complexes inside the nucleus and the counterstaining experiment with a mito-tracker did not highlight a significant uptake of the **azaBODI-Au-1** in mitochondria (Figure 8B).

### ***In vivo* investigation**

After these promising *in vitro* results, we decided to investigate the most promising complex *in vivo*. Our choice fell on **azaBODI-Au-1**, which offered the best compromise between biological activity and imaging properties.

First, the stability of **azaBODI-Au-1** was studied in DMSO, known to be a very coordinating solvent, and in the presence of phosphate buffer (PBS). This experiment was monitored by NMR (Figure 9 and Figures S11-S14). The  $^1\text{H}$ -NMR enables to have information on the stability of the overall molecule and the  $^{31}\text{P}$ -NMR enables to ensure the stability of the “P-Au” part. This follow-up, carried out over one week, shows without ambiguity that **azaBODI-Au-1** is perfectly stable in DMSO and in the presence of PBS.

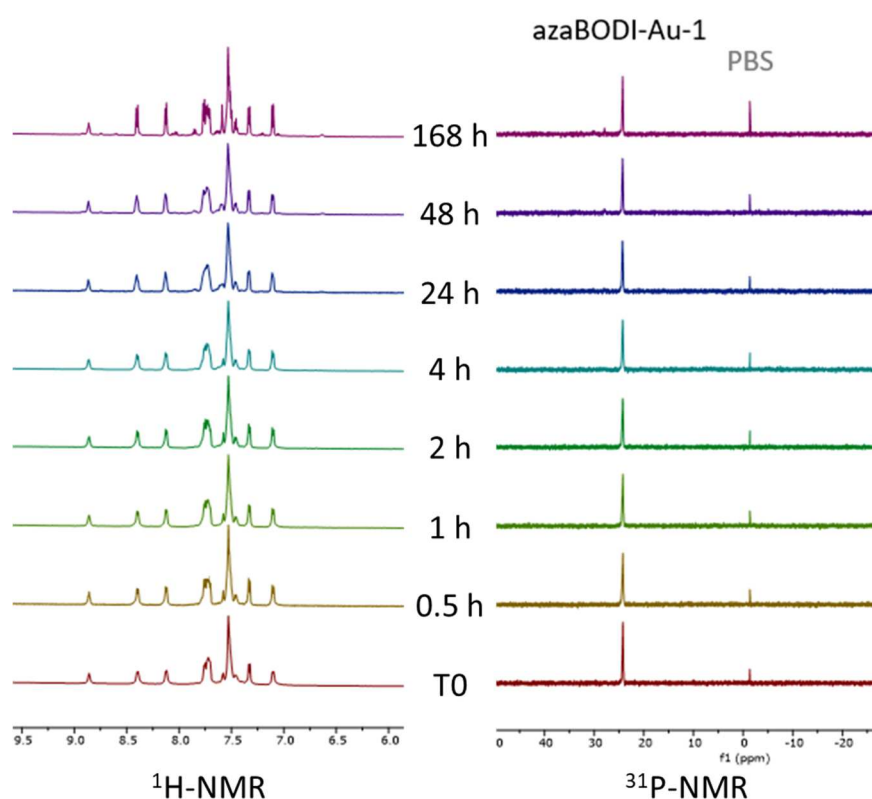


**Figure 9:** NMR stability study of **azaBODI-Au-1** in DMSO/PBS solution.

The anticancer activity of **azaBODI-Au-1** was then evaluated on BALB/c mice bearing syngenic colon CT26 flank tumors. Twice a week, **azaBODI-Au-1** was injected intravenously into the mice at a concentration of 0.5 mg/kg. Interestingly, the decrease of the tumor growth was observed within a few days after the first injection and continued all along the study (Figure 10). It is worth noting that no sign of acute toxicity (no loss of weight, no signs of pain) was detected all along the treatment duration.

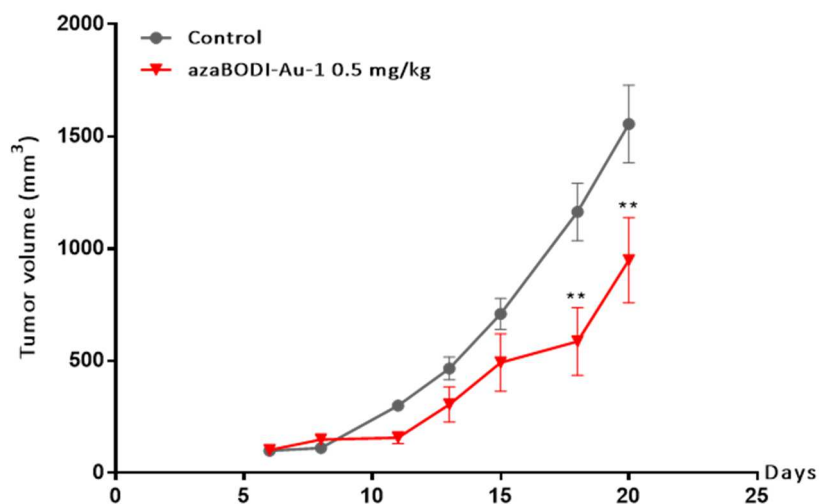


**Figure 10:** Anti-tumor effect of **azaBODI-Au-1**. Tumor-bearing BALB/c mice (n=6/group) were treated intravenously twice per week with 0.5 mg/kg of **azaBODI-Au-1** (in DMSO) or with the same quantity of DMSO (control). Tumor growth was determined 3 times per week using a caliper. Results are expressed as means  $\pm$  SEM, Two-way Anova: \*\*p $\leq$ 0.01.

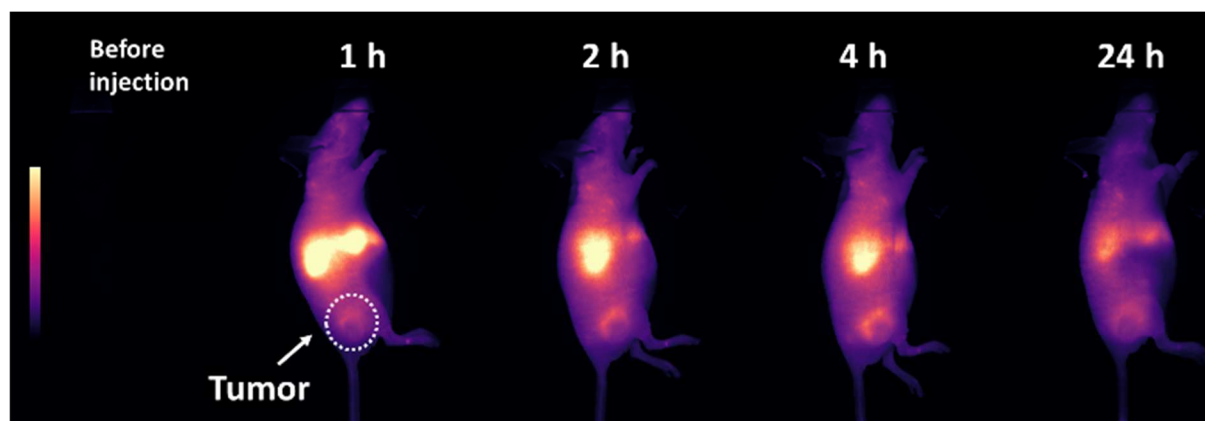


**Figure 11:** Distribution of **azaBODI-Au-1**. Tumor-bearing mice were injected intravenously and imaged before and 1, 2, 4 and 24 h after injection. The compound accumulated in the tumor area as indicated by the arrow, and was eliminated through the liver.

These results are very good for a non-vectorized compound. Therefore, we wanted to get information on the distribution of **azaBODI-Au-1** in order to see where it was accumulating. We tracked it by optical imaging with an excitation at 685 nm and a detection at 705 nm. Even if these filters are not optimal (maximum of emission of **azaBODI-Au-1** is at  $\approx$  730 nm), **azaBODI-Au-1** is perfectly detectable and trackable in real time for at least 24 h, which proves the good stability of our compound (Figure 11). Interestingly, the compound accumulated at the tumor site with a maximum around 4 hours after injection, which can explain the anticancer activity detected previously. Additionally, a strong accumulation in the liver can be noticed, which is usual for relatively lipophilic compounds, such as molecules containing organic fluorophores. It can be noted that the tumor-to-skin ratio of the theranostic compound is relatively stable over time (Figure 12). The distribution profile (Figure 12B) indicated a major hepatic elimination, while a part of the small compound is washed out through the kidney route. This is in accordance with the relatively small size of **azaBODI-Au-1**, for which the hydrodynamic radius was evaluated at 1.2 nm, i.e. below the size threshold for the renal filtration. This suggests that the compound, once internalized inside the tumor, remains

trapped in it, while it is gradually excreted from the liver and the kidneys. Moreover, the tumor-to-muscle ratio is almost 5 (Figure 12).

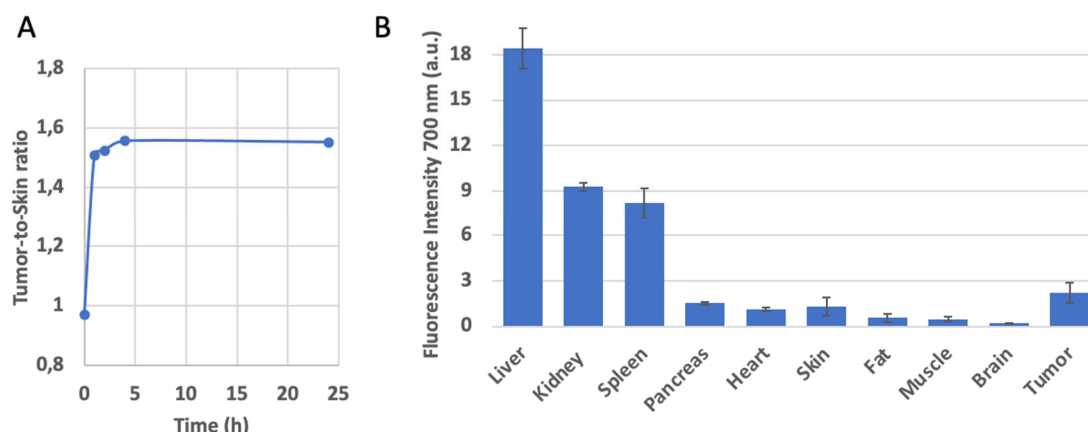


**Figure 12:** Tumor-to-skin ratio (T/S) determined *in vivo* by optical imaging (left). Distribution profile of **azaBODI-Au-1** in mice-bearing tumor, 24 h after intravenous administration (right).

## Conclusions

We reported the efficient synthesis of the first gold-based aza-BODIPY theranostics. The three homobimetallic complexes display interesting photophysical properties: absorption and emission maximal wavelengths in the NIR-I region, and good quantum yields up to ~30%. The *in vitro* results are very promising. The three gold-based aza-BODIPY have retained excellent anti-proliferative properties despite the presence of the fluorescence probe, which is not the case for the most of the reported optical based theranostic agents.[4,7,52–54] Indeed, they displayed  $IC_{50}$  in the micromolar range. They also showed a very good ability to inhibit TrxRs, in particular **azaBODI-Au-1**. In addition, the fluorescence properties of the aza-BODIPY platform were preserved and allowed a localization of the compounds by confocal imaging (they enter the cells and accumulate into cytoplasmic vesicles). Interestingly, the most active (cytotoxicity and TrxR inhibition) aza-BODIPY theranostic, **azaBODI-Au-1**, induced a very significant anti-cancer effect *in vivo* and can be tracked *in vivo* with optical imaging modalities. It is interesting to note that these very good results were obtained despite a limited accumulation of the anti-cancer agent within the tumor, the compound going mostly in the liver. This suggests that the grafting of a vector on this type of platform would dramatically increase their efficiency, which should be confirmed in next studies. All these results are very promising for future *in vivo* investigations and open the door of a novel class of powerful optical theranostic agents.

## EXPERIMENTAL

### Material and methods

Unless stated otherwise reactions were carried out in HPLC grade solvents under normal atmosphere. Solvents were purchased from BioSolve. Dry solvents were non-stabilized, purchased from Carlo Erba and dried using a MB-SPS-800 (MBraun) or PureSolv-MD-5 (Inert®). **Wazaby7** was synthesized adapting to the procedure, we reported previously.[40,44] All reagents were purchased from Sigma-Aldrich, Alfa Aesar, TCI or ACROS Organics™ and used as received without further purification. Column chromatography was carried out using alumina gel (Alfa Aesar; aluminum oxide, activated, neutral, Brockmann Grade II). Analytical thin-layer chromatography experiments were performed with Machery-Nagel Alugram Alox N/UV254 aluminum gel (precoated aluminum sheets, 0.2 mm thick). Reactions were monitored by thin-layer chromatography, RP-HPLC-MS and no-lock

<sup>31</sup>P-NMR. (<sup>1</sup>H, <sup>13</sup>C, <sup>11</sup>B, <sup>31</sup>P) were recorded at 300K (unless otherwise specified) on Bruker 500 Avance III or Bruker Avance III HD 600 MHz spectrometers (equipped with double resonance broad band probes). Chemical shifts are given relative to TMS (<sup>1</sup>H, <sup>13</sup>C), BF<sub>3</sub>·Et<sub>2</sub>O (<sup>11</sup>B) and H<sub>3</sub>PO<sub>4</sub> (<sup>31</sup>P) and were referenced to the residual solvent signal. High resolution mass spectra were recorded on a Thermo LTQ Orbitrap XL ESI-MS spectrometer. NMR and Mass-analyses were performed at the "Plateforme d'Analyse Chimique et de Synthèse Moléculaire de l'Université de Bourgogne" (PACSMUB).

## Synthesis of the ligand precursor 4

### Wazaby7

In a round-bottom flask, aza-BODIPY **2** (250 mg, 370 μmol, 1 eq) was dissolved in THF (35 mL) and deionized water (10 mL). Sodium bicarbonate (154 mg, 1.83 mmol, 5 eq) and 4-(bromomethyl)benzoic acid (173 mg, 80 μmol, 2.2 eq) were then added and the mixture was stirred at room temperature (15-20 °C) for 5 h. 4-(bromomethyl)benzoic acid was then removed *via* extraction using diethyl ether and water. The aqueous phase was concentrated under reduced pressure and HCl 3 M was added until precipitation. After centrifugation, the solid was dried under reduced pressure to finally give **Wazaby7** as a green solid (270 mg, 68% yield).

HR-MS (ESI): calcd for C<sub>60</sub>H<sub>56</sub>B<sub>1</sub>N<sub>5</sub>O<sub>6</sub><sup>2+</sup> [M]<sup>2+</sup> 476.71563 Th; found 476.71604 Th (error: 0.860 ppm). <sup>1</sup>H NMR (600 MHz, MeOD-d<sub>4</sub>): δ (ppm) = 2.87 (s, 12H), 3.83 (s, 6H), 3.95 (s, 4H), 4.26 (s, 4H), 7.15 (d, *J* = 8.7 Hz, 4H), 7.43-7.54 (m, 12H), 8.04 (d, *J* = 8.0 Hz, 4H), 8.15 (d, *J* = 7.4 Hz, 4H), 8.46 (d, *J* = 8.7 Hz, 4H). <sup>13</sup>C NMR (151 MHz, MeOD-d<sub>4</sub>): δ (ppm) = 50.7, 55.5, 56.2, 66.7, 88.4, 115.3, 121.3, 125.4, 128.9, 129.7, 129.8, 130.4, 130.7, 131.1, 131.5, 132.7, 133.4, 133.9, 134.0, 134.1, 134.5, 144.1, 144.2, 159.0, 163.7, 168.5. <sup>11</sup>B NMR (192 MHz, MeOD-d<sub>4</sub>): δ (ppm) = -12.36. LogP approximation: LogD = 1.36. Counter-anions have been checked by ion chromatography. Only chlorides were detected.

### AzaBODI-Au-1

In a round-bottom flask, **Wazaby7** (45 mg, 40 μmol) was dissolved in anhydrous DMF (4 mL). A solution of HBTU (34 mg, 89 μmol, 2.2 eq) in anhydrous DMF (5 mL) was added, followed by an addition of DIPEA (56 μL, 323 μmol, 8 eq). After stirring at room temperature (≈ 20-25 °C) for 15 min, a solution of 2-(diphenylphosphino)ethylamine-aurochloride (37 mg, 80 μmol, 2 eq) in DMF (5 mL) was added to the mixture. After 4 h, TLC confirmed complete conversion of the reagent. The solvents were removed under reduced pressure and the crude product was purified on alumina column (DCM to DCM/MeOH 96/4). After removal of the solvents under reduced pressure, the product underwent ion exchange (Amberlite IRA-410, ACN/water 1:1). The solid was precipitated from DCM using diethyl ether to give **azaBODI-Au-1** (67 mg, 82% yield) as a green solid.

R<sub>f</sub> (alumina, DCM/MeOH 9:1) = 0.5. HR-MS (ESI): calcd for C<sub>88</sub>H<sub>84</sub>Au<sub>2</sub>BCl<sub>2</sub>N<sub>7</sub>O<sub>4</sub>P<sub>2</sub>-2HCl<sup>2+</sup> [M-2HCl]<sup>2+</sup> 883.76583 Th; found 883.76766 Th (error: 2.071 ppm). <sup>1</sup>H NMR (600 MHz, DMSO-d<sub>6</sub>): δ (ppm) = 2.77 (s, 12H), 3.05-3.09 (m, 4H), 3.50-3.55 (m, 4H), 3.77 (s, 6H), 3.98 (s, 4H), 4.21 (s, 4H), 7.14 (d, *J* = 8.5 Hz, 4H), 7.37 (d, *J* = 8.5 Hz, 4H), 7.48 (t, *J* = 7.3 Hz, 2H), 7.52-7.59 (m, 16H), 7.66 (s, 2H), 7.78 (ddd, *J* = 12.9, 7.5, 1.8 Hz, 8H), 7.82 (d, *J* = 7.9 Hz, 4H), 8.17 (d, *J* = 7.1 Hz, 4H), 8.45 (d, *J* = 8.5 Hz, 4H), 8.85 (t, *J* = 5.4 Hz, 2H, NH). <sup>13</sup>C NMR (151 MHz, DMSO-d<sub>6</sub>): δ (ppm) = 14.0, 15.2, 18.8, 26.3 (d, *J*<sub>C-P</sub> = 37.8 Hz), 26.6, 30.4, 34.4, 35.5, 49.2, 53.8, 55.6, 64.8, 64.9, 87.1, 114.1, 120.8, 123.4, 124.9, 127.8, 128.9 (d, *J*<sub>C-P</sub> = 46.1 Hz), 128.9, 129.3, 129.4 (d, *J*<sub>C-P</sub> = 11.6 Hz), 130.1, 131.7, 132.1, 132.3, 132.7, 133.1 (d, *J*<sub>C-P</sub> = 13.1 Hz), 135.5, 139.2, 141.3, 142.3, 157.1, 161.7, 165.3. <sup>31</sup>P NMR (193 MHz, DMSO-d<sub>6</sub>): δ (ppm) = 24.6. LogP approximation: LogD = 3.81. Counter-anions have been checked by ion chromatography. Only chlorides were detected.

### AzaBODI-Au-2

In a Schlenk tube, 2-(dimethylamino)ethanethiol hydrochloride (10 mg, 73 μmol, 2.1 eq) was solubilized in 15 mL of anhydrous DCM. Anhydrous DIPEA (60 μL, 10 eq.) was added and the

suspension was stirred in the dark under argon at 20 °C for 10 minutes. In a second Schlenk tube, **azaBODI-Au-1** (70 mg, 35 μmol) was dissolved in 35 mL of anhydrous DCM. The solution was stirred at 0 °C for 5 minutes. The suspension from the first Schlenk tube was then slowly added *via* canula to the second Schlenk tube in the dark at 0 °C. The mixture was then stirred at room temperature (≈ 20 °C) for 18 h. 2-(dimethylamino)ethanethiol hydrochloride (6 mg, 42 μmol, 1.2 eq.) and anhydrous DIPEA (60 μL, 10 eq.) dissolved in anhydrous DCM (2 mL) were added and the mixture was stirred for 2 additional hours. After completion (monitored by TLC), the solvents were removed under reduced pressure, and the residue was purified by alumina gel chromatography (eluent DCM to DCM/MeOH 97/3). Ion exchange was performed (Amberlite IRA-410, ACN/water 1:1) and after removal of the solvents under reduced pressure, the solid was precipitated from DCM using diethyl ether to give **azaBODI-Au-2** (50 mg, 63% yield) as a green powder.

R<sub>f</sub> (alumina, DCM/MeOH 9:1) = 0.3. <sup>1</sup>H-NMR (600 MHz, 318 K, DMSO-d<sub>6</sub>): δ (ppm) = 2.08 (s, 12H), 2.45 (t, *J* = 5.5 Hz, 4H), 2.77 (s, 12H), 2.91 (t, *J* = 7.2 Hz, 4H), 2.98-3.02 (m, 4H), 3.52-3.58 (m, 4H), 3.70-3.80 (m, 6H), 3.97 (s, 4H), 4.19 (s, 4H), 7.00-8.82 (m, 50H, H<sub>arom</sub>, NH). <sup>31</sup>P-NMR (243 MHz, 328 K, DMSO-d<sub>6</sub>): δ (ppm) = 28.2 (broad). LogP approximation: LogD = 1.44. Counter-anions have been checked by ion chromatography. Only chlorides were detected.

### AzaBODI-Au-3

In a Schlenk tube, sodium 2-mercaptoethanesulfonate (5.4 mg, 33 μmol, 2.2 eq.) were suspended in 3.5 mL of degassed acetone and a solution of 0.1 M NaOH (150 μL, 1 eq.) were added. The suspension was stirred in the dark under argon at 10-15 °C for 10 minutes. In a second Schlenk tube, **azaBODI-Au-1** (30 mg, 15 μmol) was solubilized in 4 mL of degassed acetone. The solution was stirred at 0 °C for 5 minutes. The suspension from the first Schlenk tube was then slowly added *via* canula to the second Schlenk tube in the dark. The mixture was then stirred at 12 °C for 3 h. After completion monitored by <sup>31</sup>P-NMR, the crude product was evaporated to dryness, solubilized in a dichloromethane/methanol mixture, then filtrated to remove uncolored particles. Ion exchange was performed (Amberlite IRA-410, ACN/water 1:1). The product was obtained after complete evaporation to give **azaBODI-Au-3** (15 mg, 44% yield) as a green powder.

HR-MS (ESI): calcd for C<sub>92</sub>H<sub>92</sub>Au<sub>2</sub>BN<sub>7</sub>O<sub>10</sub>P<sub>2</sub>S<sub>4</sub>-C<sub>2</sub>H<sub>4</sub>O<sub>3</sub>S<sub>2</sub><sup>2+</sup> [M-C<sub>2</sub>H<sub>4</sub>O<sub>3</sub>S<sub>2</sub>]<sup>2+</sup> 954.75375 Th; found 954.751919 Th (error: -1.927 ppm). <sup>1</sup>H NMR (600 MHz, DMSO-d<sub>6</sub>): δ (ppm) = 2.68-2.73 (m, 4H), 2.77 (s, 12H), 3.01-3.06 (m, 4H), 3.06-3.12 (m, 4H), 3.52-3.60 (m, 4H), 3.73 (s, 6H), 4.02 (s, 4H), 4.22 (s, 4H), 7.17 (d, *J* = 8.5 Hz, 4H), 7.44 (d, *J* = 7.9 Hz, 4H), 7.48-7.57 (m, 18H), 7.67 (s, 2H), 7.76-7.84 (m, 8H), 7.91 (d, *J* = 7.8 Hz, 4H), 8.18 (d, *J* = 7.5 Hz, 4H), 8.48 (d, *J* = 8.4 Hz, 4H), 8.98 (s, 2H, NH). <sup>13</sup>C NMR (151 MHz, DMSO-d<sub>6</sub>): δ (ppm) = 14.0, 16.7, 18.0, 18.8, 19.9, 22.1, 23.8, 26.4-26.6(m), 28.4-29.1 (m), 30.4, 30.7, 31.3, 32.6, 33.7, 33.9, 35.1, 35.4, 48.6, 49.2, 51.3, 54.1, 54.9, 55.3, 55.7, 59.7, 64.9, 69.8, 87.1, 114.2, 120.8, 123.4, 127.8, 128.8-129.1 (d, *J*<sub>C13'-P</sub> = 50.7 Hz), 128.9, 129.3-129.4 (m), 129.5, 129.7, 130.0, 130.3, 131.7, 131.8, 132.5, 132.8, 133.1, 133.2 (d, *J*<sub>C15'-P</sub> = 13.2 Hz), 135.5, 141.2, 142.3, 157.1, 161.7, 165.3, 174.5. <sup>31</sup>P-NMR (202 MHz, DMSO-d<sub>6</sub>): δ (ppm) = 25.4 (broad). Counter-anions have been checked by ion chromatography. Only chlorides were detected.

### FCS analysis (hydrodynamic radius)

FCS study was performed using a confocal laser-scanning microscope (LSM 710 Carl Zeiss, Jena, Germany) with a 40× water immersion C-Apochromat objective lens (numerical aperture (N.A.) = 1.2). The measurements were carried out at room temperature in 8-well Lab-Tek I chambered coverglass (Nalge Nunc International, Illkirch, France). The 633 nm He-Ne laser beam was focused into 20 μL solutions at 100 μm over the cover glass. The fluorescence emission was collected through a pinhole and a 650 nm-long pass filter. Photon counts were detected by an Avalanche PhotoDiode at 20 MHz for 30 seconds, and repeated 10 times in triplicates. The data evaluation was performed using the Zeiss FCS Fit software (Zeiss, Jena, Germany). The intensity autocorrelation curves were

fitted using a free diffusion model with one component. A preliminary calibration step with Cy5 made it possible to evaluate the size of the confocal volume ( $\approx 1$  fL). The hydrodynamic radius was calculated using the Stokes-Einstein equation.

## **Biological experimental procedures**

### **Cell culture**

Mouse and human breast (4T1 and MDA-MB-231 respectively) and colon (CT26 and SW480 respectively) cancer cell lines, were cultured in RPMI supplemented with 10 % FBS. All the cells were cultured at 37 °C under a humidified atmosphere containing 5 % CO<sub>2</sub>. The cells were detached by trypsin and re-seeded at least 1 day before any experiment.

### ***In vitro* confocal imaging**

MDA-MB-231 and 4T1 cells were plated in 4-well Lab-Tek I Chamber slide (Nunc™, Thermo Scientific) (50,000 cells in 500  $\mu$ L of culture medium) and incubated overnight in RPMI without red phenol medium at 37 °C and 5% CO<sub>2</sub>. Uptake experiments were performed by incubating cells with the different theranostic compounds (5  $\mu$ M) at 37 °C and 5 % CO<sub>2</sub>. For confocal imaging, live cells were scanned by confocal microscopy (Zeiss LMS510 microscope) using a 63x oil immersion objective of 1.2 numerical aperture. Hoechst 33342 was used to label the nucleus (0.5  $\mu$ M), excited at 405 nm (2-5%) and its signal was collected from 410 to 499 nm. The theranostic compounds were excited at 633 nm (2% power) and the signal was collected from 640 to 747 nm. Images were processed with ImageJ software.

### **FACS experiment**

Similar protocol was observed for FACS experiment, with a 15 min to 24 h incubation with 5  $\mu$ M theranostic solution. After washing with PBS, the cells were observed using LSR II (Becton, Dickinson and Company, Pont de Claix, France). Cells were gated to exclude cell debris in the control group and 50,000 events were recorded in the gate for fluorescence intensity measurement.

### **Determination of cytotoxic properties**

10<sup>5</sup> cells were seeded in 96-well flat-bottomed microplates (final volume 100  $\mu$ L per well) and incubated for 24h to allow for cell adherence. 10 mM stock solutions were prepared by dissolving the compounds in DMSO. Fresh medium containing increasing concentrations of the compounds (ranging from 0.01 to 25  $\mu$ M) was added and plates were incubated at 37 °C for 48 h. The cytotoxic activity of compounds and drug references was determined using the MTS assay (Promega®). The assay is based on the reduction of a tetrazolium compound to a colored formazan in the presence of an electron coupling reagent (phenazine ethosulfate; PES) and NADH/NADPH produced by metabolically active cells. Thereafter, 20  $\mu$ L of MTS (3-(4,5-dimethylthiazol-2-yl)-5-(3-carboxymethoxy phenyl)-2-(4-sulfophenyl)-2H-tetrazolium, Promega, Charbonnières, France) was added in each wells and absorbance at 490 nm was measured after 3h incubation at 37 °C. The resulting IC<sub>50</sub> values were calculated using GraphPad Prism 5.0 software. Each treatment was performed in three independent experiments.

### **Thioredoxin reductase (TrxRs) activity assay**

TrxRs assays were carried out on CT26 cells incubated during 24h in RPMI medium containing 10% FBS with 5  $\mu$ M of azaBODI-Au-1, azaBODI-Au-2, azaBODI-Au-3 or auranofin. Cells were scratched from the bottom of the dish after a washing step in PBS. Cell pellets were resuspended in 50  $\mu$ L of a lysis buffer CellLytic-M (Sigma-Aldrich) during 15 min, and centrifugated at 16,000g for 10 min at 4 °C. The supernatants were transferred to 96-well microplates for protein dosage. The protein concentrations in the cell homogenates were determined by the Lowry method thanks to a protein Assay Reagents Package Kit (Bio-Rad). From each homogenate 20  $\mu$ g protein were collected for The

TrxRs enzyme activity measurement with a commercially available kit (Sigma-Aldrich). The assay is based on the reduction of 5,5'-dithiobis(2-nitrobenzoic acid) (DTNB) with NADPH to 5-thio-2-nitrobenzoic acid (TNB) by TrxRs. The yellow color product is measurable at 412 nm by spectrophotometry. The reaction was performed in a working buffer (100 mM potassium phosphate with 10 mM EDTA and 0.24 mM NADPH) in a final volume of 200  $\mu$ L. This reaction was initiated by the addition of 6  $\mu$ L DTNB (39.6 mg/mL) diluted in an assay buffer (6 M guanidine-HCl in 0.2 M Tris-HCl, pH 8.0). The absorbance at 412 nm was measured 18 times within 15 min on a Perkin Elmer Wallac 1420 Victor2 Microplate Reader. The same experiments were performed for each condition with a specific inhibitor of TrxRs. The TrxRs activity rate was calculated from the slope of absorbance at 412 nm versus time after the subtraction of the activity measured in presence of the inhibitor.

### ***In vivo* experiments guidelines**

All experiments followed the guidelines of the Federation of European Animal Science Associations and were all approved by the Ministry of agriculture and food (France, Apafis number: #8782 and Apafis number: #15181) and by respectively the Ethics Committee of Grenoble Alpes University (Grenoble, France) and the Ethics Committee of Burgundy University (Dijon, France).

### **Determination of the anti-tumor effect**

In order to test the potential anti-tumor effect of **azaBODI-Au-1**, BALB/c mice (8 weeks old, Charles River, France) were grafted by subcutaneous injection of murine colon cancer CT26 cells ( $5 \cdot 10^5$  cells). Seven days after tumor implantation (tumor volume around 50 mm<sup>3</sup>), tumor-bearing mice were randomized into two groups, one received 0.5 mg/kg of **azaBODI-Au-1** (in DMSO) and the other received the same quantity of DMSO in saline (Control) by intravenous injection (IV) in the vein tail. These IV injections were performed two times a week and tumor volume assessed three times per week. Mice whose tumor reached 1,500 mm<sup>3</sup> were euthanized due to ethical reasons.

### ***In vivo* optical imaging**

**azaBODI-Au-1** distribution was determined on mice bearing sub-cutaneous 4T1 tumor cells. NMRI mice (6 weeks old, Janvier, France) were injected with  $1 \cdot 10^6$  cells, and imaged when the tumors reached >300 mm<sup>3</sup> (*i.e.* 2 weeks). Mice were imaged before and after injection of 50  $\mu$ g of **azaBODI-Au-1**, at 1, 2, 4 and 24 h using LI-COR Pearl Trilogy system (LI-COR, Germany) at 700 nm. Organs were imaged at the end of the experiment in the same conditions.

### **Conflicts of interest**

“There are no conflicts to declare”.

### **Acknowledgements**

The Ministère de l'Enseignement Supérieur et de la Recherche, the Centre National de la Recherche Scientifique (CNRS), the Conseil Régional de Bourgogne (PhD JCE grant # 2015-9205AAO033S04139 / BG0003203 and # 2018Y-08158), and the French Research National Agency (ANR) via project JCJC “SPID” ANR-16-CE07-0020 and project JCJC “WazaBY” ANR-18-CE18-0012 are gratefully acknowledged. This work is part of the projects “Pharmaco-imagerie et agents théranostiques” et “Chimie durable, environnement et agroalimentaire” supported by the Université de Bourgogne and the Conseil Régional de Bourgogne through the Plan d'Actions Régional pour l'Innovation (PARI) and the European Union through the PO FEDER-FSE Bourgogne 2014/2020 programs. This work was also partially supported by grants from Ligue contre le Cancer, Comité de Côte d'Or. Prof. Anthony Romieu, FrenchBIC, GDR AIM, and OncoDesign® are acknowledged for fruitful discussion. Dr Picquet, Dr Bonnin, and Ms M.-J. Penouilh are gratefully acknowledged for HR-MS, NMR analyses, Dr Myriam Laly for ionic chromatography and Valérie Saint-Giorgio (zootechny center, UBFC)

## Notes and references

- [1] C. Yan, Y. Zhang, Z. Guo, Recent progress on molecularly near-infrared fluorescent probes for chemotherapy and phototherapy, *Coordination Chemistry Reviews*. 427 (2021) 213556. <https://doi.org/10.1016/j.ccr.2020.213556>.
- [2] I. Velikyan, (Radio)Theranostic Patient Management in Oncology Exemplified by Neuroendocrine Neoplasms, Prostate Cancer, and Breast Cancer, *Pharmaceuticals*. 13 (2020) 39. <https://doi.org/10.3390/ph13030039>.
- [3] I.J. Pruis, G.A.M.S. van Dongen, S.E.M. Veldhuijzen van Zanten, The Added Value of Diagnostic and Theranostic PET Imaging for the Treatment of CNS Tumors, *IJMS*. 21 (2020) 1029. <https://doi.org/10.3390/ijms21031029>.
- [4] J. Pliquett, S. Amor, M. Ponce-Vargas, M. Laly, C. Racœur, Y. Rousselin, F. Denat, A. Bettaieb, P. Fleurat-Lessard, C. Paul, C. Goze, E. Bodio, Design of a multifunctionalizable BODIPY platform for the facile elaboration of a large series of gold(I)-based optical theranostics, *Dalton Trans.* (2018). <https://doi.org/10.1039/C8DT02364F>.
- [5] Y. Yuan, R.T.K. Kwok, B.Z. Tang, B. Liu, Targeted Theranostic Platinum(IV) Prodrug with a Built-In Aggregation-Induced Emission Light-Up Apoptosis Sensor for Noninvasive Early Evaluation of Its Therapeutic Responses in Situ, *J. Am. Chem. Soc.* 136 (2014) 2546–2554. <https://doi.org/10.1021/ja411811w>.
- [6] M. Redrado, V. Fernández-Moreira, M.C. Gimeno, Theranostics Through the Synergistic Cooperation of Heterometallic Complexes, *ChemMedChem*. 16 (2021) 932–941. <https://doi.org/10.1002/cmdc.202000833>.
- [7] B. Bertrand, K. Passador, C. Goze, F. Denat, E. Bodio, M. Salmain, Metal-based BODIPY derivatives as multimodal tools for life sciences, *Coordination Chemistry Reviews*. 358 (2018) 108–124. <https://doi.org/10.1016/j.ccr.2017.12.007>.
- [8] A. Luengo, V. Fernández-Moreira, I. Marzo, M.C. Gimeno, Bioactive Heterobimetallic Re(I)/Au(I) Complexes Containing Bidentate N-Heterocyclic Carbenes, *Organometallics*. 37 (2018) 3993–4001. <https://doi.org/10.1021/acs.organomet.8b00601>.
- [9] V. Fernández-Moreira, M.C. Gimeno, Heterobimetallic Complexes for Theranostic Applications, *Chemistry – A European Journal*. 24 (2018) 3345–3353. <https://doi.org/10.1002/chem.201705335>.
- [10] A. Trommenschlager, F. Chotard, B. Bertrand, S. Amor, P. Richard, A. Bettaieb, C. Paul, J.-L. Connat, P. Le Gendre, E. Bodio, Gold(I)–Coumarin–Caffeine-Based Complexes as New Potential Anti-Inflammatory and Anticancer Trackable Agents, *ChemMedChem*. 13 (2018) 2408–2414. <https://doi.org/10.1002/cmdc.201800474>.
- [11] A. Luengo, V. Fernández-Moreira, I. Marzo, M.C. Gimeno, Trackable Metallodrugs Combining Luminescent Re(I) and Bioactive Au(I) Fragments, *Inorg. Chem.* 56 (2017) 15159–15170. <https://doi.org/10.1021/acs.inorgchem.7b02470>.
- [12] M. Wenzel, A. de Almeida, E. Bigaeva, P. Kavanagh, M. Picquet, P. Le Gendre, E. Bodio, A. Casini, New Luminescent Polynuclear Metal Complexes with Anticancer Properties: Toward Structure–Activity Relationships, *Inorg. Chem.* 55 (2016) 2544–2557. <https://doi.org/10.1021/acs.inorgchem.5b02910>.
- [13] L. Dondaine, D. Escudero, M. Ali, P. Richard, F. Denat, A. Bettaieb, P. Le Gendre, C. Paul, D. Jacquemin, C. Goze, E. Bodio, Coumarin-Phosphine-Based Smart Probes for Tracking Biologically Relevant Metal Complexes: From Theoretical to Biological Investigations, *Eur. J. Inorg. Chem.* 2016 (2016) 545–553. <https://doi.org/10.1002/ejic.201501304>.
- [14] B. Bertrand, P.-E. Doulain, C. Goze, E. Bodio, Development of trackable metal-based drugs: new generation of therapeutic agents, *Dalton Trans.* 45 (2016) 13005–13011. <https://doi.org/10.1039/C5DT04275E>.

- [15] R. Visbal, V. Fernández-Moreira, I. Marzo, A. Laguna, M.C. Gimeno, Cytotoxicity and biodistribution studies of luminescent Au(I) and Ag(I) N-heterocyclic carbenes. Searching for new biological targets, *Dalton Trans.* 45 (2016) 15026–15033. <https://doi.org/10.1039/C6DT02878K>.
- [16] P.-E. Doulain, R. Decréau, C. Racœur, V. Goncalves, L. Dubrez, A. Bettaieb, P.L. Gendre, F. Denat, C. Paul, C. Goze, E. Bodio, Towards the elaboration of new gold-based optical theranostics, *Dalton Trans.* 44 (2015) 4874–4883. <https://doi.org/10.1039/C4DT02977A>.
- [17] S. Tasan, O. Zava, B. Bertrand, C. Bernhard, C. Goze, M. Picquet, P. Le Gendre, P. Harvey, F. Denat, A. Casini, E. Bodio, BODIPY–phosphane as a versatile tool for easy access to new metal-based theranostics, *Dalton Trans.* 42 (2013) 6102–6109. <https://doi.org/10.1039/C2DT32055J>.
- [18] A. Citta, E. Schuh, F. Mohr, A. Folda, M.L. Massimino, A. Bindoli, A. Casini, M.P. Rigobello, Fluorescent silver(i) and gold(i)–N-heterocyclic carbene complexes with cytotoxic properties: mechanistic insights, *Metallomics.* 5 (2013) 1006. <https://doi.org/10.1039/c3mt20260g>.
- [19] G. Gupta, P. Kumari, J.Y. Ryu, J. Lee, S.M. Mobin, C.Y. Lee, Mitochondrial Localization of Highly Fluorescent and Photostable BODIPY-Based Ruthenium(II), Rhodium(III), and Iridium(III) Metal Complexes, *Inorg. Chem.* 58 (2019) 8587–8595. <https://doi.org/10.1021/acs.inorgchem.9b00898>.
- [20] A. Trommenschlager, F. Chotard, B. Bertrand, S. Amor, L. Dondaine, M. Picquet, P. Richard, A. Bettaieb, P.L. Gendre, C. Paul, C. Goze, E. Bodio, Gold(I)–BODIPY–imidazole bimetallic complexes as new potential anti-inflammatory and anticancer trackable agents, *Dalton Trans.* (2017). <https://doi.org/10.1039/C7DT01377A>.
- [21] J. Ceramella, A. Mariconda, D. Iacopetta, C. Saturnino, A. Barbarossa, A. Caruso, C. Rosano, M.S. Sinicropi, P. Longo, From coins to cancer therapy: Gold, silver and copper complexes targeting human topoisomerases, *Bioorganic & Medicinal Chemistry Letters.* 30 (2020) 126905. <https://doi.org/10.1016/j.bmcl.2019.126905>.
- [22] C. Yeo, K. Ooi, E. Tiekink, Gold-Based Medicine: A Paradigm Shift in Anti-Cancer Therapy?, *Molecules.* 23 (2018) 1410. <https://doi.org/10.3390/molecules23061410>.
- [23] A. Sigel, H. Sigel, E. Freisinger, R.K.O. Sigel, eds., *Metallo-Drugs: Development and Action of Anticancer Agents*, De Gruyter, Berlin, Boston, 2018. <https://doi.org/10.1515/9783110470734>.
- [24] B. Bertrand, M.R.M. Williams, M. Bochmann, Gold(III) Complexes for Antitumor Applications: An Overview, *Chem. Eur. J.* 24 (2018) 11840–11851. <https://doi.org/10.1002/chem.201800981>.
- [25] C. Nardon, N. Pettenuzzo, D. Fregona, Gold Complexes for Therapeutic Purposes: an Updated Patent Review (2010–2015), *CMC.* 23 (2016) 3374–3403. <https://doi.org/10.2174/0929867323666160504103843>.
- [26] T. Zou, C.T. Lum, C.-N. Lok, J.-J. Zhang, C.-M. Che, Chemical biology of anticancer gold(III) and gold(I) complexes, *Chem. Soc. Rev.* 44 (2015) 8786–8801. <https://doi.org/10.1039/C5CS00132C>.
- [27] B.Đ. Glišić, M.I. Djuran, Gold complexes as antimicrobial agents: an overview of different biological activities in relation to the oxidation state of the gold ion and the ligand structure, *Dalton Trans.* 43 (2014) 5950–5969. <https://doi.org/10.1039/C4DT00022F>.
- [28] X. Zhang, K. Selvaraju, A.A. Saei, P. D’Arcy, R.A. Zubarev, E.S.J. Arnér, S. Linder, Repurposing of auranofin: Thioredoxin reductase remains a primary target of the drug, *Biochimie.* 162 (2019) 46–54. <https://doi.org/10.1016/j.biochi.2019.03.015>.
- [29] E.V. Capparelli, R. Bricker-Ford, M.J. Rogers, J.H. McKerrow, S.L. Reed, Phase I Clinical Trial Results of Auranofin, a Novel Antiparasitic Agent, *Antimicrobial Agents and Chemotherapy.* 61 (2017). <https://doi.org/10.1128/AAC.01947-16>.
- [30] L.R.A. James, Z.-Q. Xu, R. Sluyter, E.L. Hawksworth, C. Kelso, B. Lai, D.J. Paterson, M.D. de Jonge, N.E. Dixon, J.L. Beck, S.F. Ralph, C.T. Dillon, An investigation into the interactions of gold nanoparticles and anti-arthritis drugs with macrophages, and their reactivity towards thioredoxin reductase, *Journal of Inorganic Biochemistry.* 142 (2015) 28–38. <https://doi.org/10.1016/j.jinorgbio.2014.09.013>.
- [31] T. Onodera, I. Momose, M. Kawada, Potential Anticancer Activity of Auranofin, *Chemical and Pharmaceutical Bulletin.* 67 (2019) 186–191. <https://doi.org/10.1248/cpb.c18-00767>.

- [32] T.M. Simon, D.H. Kunishima, G.J. Vibert, A. Lorber, Screening trial with the coordinated gold compound auranofin using mouse lymphocyte leukemia P388, *Cancer Res.* 41 (1981) 94–97.
- [33] O. Florès, A. Trommenschlager, S. Amor, F. Marques, F. Silva, L. Gano, F. Denat, M.P.C. Campello, C. Goze, E. Bodio, P.L. Gendre, In vitro and in vivo trackable titanocene-based complexes using optical imaging or SPECT, *Dalton Trans.* 46 (2017) 14548–14555. <https://doi.org/10.1039/C7DT01981E>.
- [34] E. Bodio, P. Le Gendre, F. Denat, C. Goze, *Advances in Inorganic Chemistry - Elsevier, Advances in Inorganic Chemistry.* 68 (2016) 253–299.
- [35] J. Pliquett, A. Dubois, C. Racœur, N. Mabrouk, S. Amor, R. Lescure, A. Bettaïeb, B. Collin, C. Bernhard, F. Denat, P.S. Bellaye, C. Paul, E. Bodio, C. Goze, A Promising Family of Fluorescent Water-Soluble aza-BODIPY Dyes for in Vivo Molecular Imaging, *Bioconjugate Chem.* 30 (2019) 1061–1066. <https://doi.org/10.1021/acs.bioconjchem.8b00795>.
- [36] B. Bertrand, A. Casini, A golden future in medicinal inorganic chemistry: the promise of anticancer gold organometallic compounds, *Dalton Trans.* 43 (2014) 4209–4219. <https://doi.org/10.1039/c3dt52524d>.
- [37] L. Ortego, F. Cardoso, S. Martins, M.F. Fillat, A. Laguna, M. Meireles, M.D. Villacampa, M.C. Gimeno, Strong inhibition of thioredoxin reductase by highly cytotoxic gold(I) complexes. DNA binding studies, *Journal of Inorganic Biochemistry.* 130 (2014) 32–37. <https://doi.org/10.1016/j.jinorgbio.2013.09.019>.
- [38] A. Godard, G. Kalot, J. Pliquett, B. Busser, X. Le Guével, K.D. Wegner, U. Resch-Genger, Y. Rousselin, J.-L. Coll, F. Denat, E. Bodio, C. Goze, L. Sancey, Water-Soluble Aza-BODIPYS: Biocompatible Organic Dyes for High Contrast In Vivo NIR-II Imaging, *Bioconjug. Chem.* 31 (2020) 1088–1092. <https://doi.org/10.1021/acs.bioconjchem.0c00175>.
- [39] G. Kalot, A. Godard, B. Busser, J. Pliquett, M. Broekgaarden, V. Motto-Ros, K.D. Wegner, U. Resch-Genger, U. Köster, F. Denat, J.-L. Coll, E. Bodio, C. Goze, L. Sancey, Aza-BODIPY: A New Vector for Enhanced Theranostic Boron Neutron Capture Therapy Applications, *Cells.* 9 (2020) 1953. <https://doi.org/10.3390/cells9091953>.
- [40] O. Florès, J. Pliquett, L. Abad Galan, R. Lescure, F. Denat, O. Maury, A. Pallier, P.-S. Bellaye, B. Collin, S. Mème, C.S. Bonnet, E. Bodio, C. Goze, Aza-BODIPY Platform: Toward an Efficient Water-Soluble Bimodal Imaging Probe for MRI and Near-Infrared Fluorescence, *Inorg Chem.* 59 (2020) 1306–1314. <https://doi.org/10.1021/acs.inorgchem.9b03017>.
- [41] Z. Shi, X. Han, W. Hu, H. Bai, B. Peng, L. Ji, Q. Fan, L. Li, W. Huang, Bioapplications of small molecule Aza-BODIPY: from rational structural design to *in vivo* investigations, *Chem. Soc. Rev.* 49 (2020) 7533–7567. <https://doi.org/10.1039/D0CS00234H>.
- [42] E. Bodio, F. Denat, C. Goze, BODIPYS and aza-BODIPY derivatives as promising fluorophores for *in vivo* molecular imaging and theranostic applications, *J. Porphyrins Phthalocyanines.* 23 (2019) 1159–1183. <https://doi.org/10.1142/S1088424619501268>.
- [43] E. Kitteringham, D. Wu, S. Cheung, B. Twamley, D.F. O’Shea, D.M. Griffith, Development of a novel carboplatin like cytoplasmic trackable near infrared fluorophore conjugate via strain-promoted azide alkyne cycloaddition, *Journal of Inorganic Biochemistry.* 182 (2018) 150–157. <https://doi.org/10.1016/j.jinorgbio.2018.02.010>.
- [44] J. Pliquett, A. Dubois, C. Racœur, N. Mabrouk, S. Amor, R. Lescure, A. Bettaïeb, B. Collin, C. Bernhard, F. Denat, P.S. Bellaye, C. Paul, E. Bodio, C. Goze, A Promising Family of Fluorescent Water-Soluble aza-BODIPY Dyes for in Vivo Molecular Imaging, *Bioconjugate Chem.* 30 (2019) 1061–1066. <https://doi.org/10.1021/acs.bioconjchem.8b00795>.
- [45] E.M. Barranco, M.C. Gimeno, P.G. Jones, A. Laguna, M.D. Villacampa, Synthesis of the Ferrocene Derivative  $\text{FcCHN}(\text{CH}_2)_2\text{SH}$  [ $\text{Fc} = (\eta^5\text{-C}_5\text{H}_5)\text{Fe}(\eta^5\text{-C}_5\text{H}_4)$ ]: Reactivity toward (Phosphine)gold(I) Cations, *Inorg. Chem.* 38 (1999) 702–706. <https://doi.org/10.1021/ic980379e>.
- [46] A. Gutiérrez, I. Marzo, C. Cativiela, A. Laguna, M.C. Gimeno, Highly Cytotoxic Bioconjugated Gold(I) Complexes with Cysteine-Containing Dipeptides, *Chem. Eur. J.* 21 (2015) 11088–11095. <https://doi.org/10.1002/chem.201501458>.

- [47] A. Miccoli, B.A. Dhiani, P.J. Thornton, O.A. Lambourne, E. James, H. Kadri, Y. Mehellou, Aryloxy Triester Phosphoramidates as Phosphoserine Prodrugs: A Proof of Concept Study, *ChemMedChem*. 15 (2020) 671–674. <https://doi.org/10.1002/cmdc.202000034>.
- [48] J. Park, J.I. Um, A. Jo, J. Lee, D.-W. Jung, D.R. Williams, S.B. Park, Impact of molecular charge on GLUT-specific cellular uptake of glucose bioprobes and in vivo application of the glucose bioprobe, GB2-Cy3, *Chem. Commun.* 50 (2014) 9251–9254. <https://doi.org/10.1039/C4CC00955J>.
- [49] P.J. Sadler, R.E. Sue, *The Chemistry of Gold Drugs, Metal-Based Drugs*. 1 (1994) 107–144. <https://doi.org/10.1155/MBD.1994.107>.
- [50] P.-E. Doulain, S. Tazan, R. Decreau, C. Paul, P. Le Gendre, F. Denat, C. Goze, E. Bodio, Toward the elaboration of new gold-based optical theranostics for in vivo imaging, *J. Biol. Inorg. Chem.* 19 (2014) S793–S793.
- [51] A.M. Brouwer, Standards for photoluminescence quantum yield measurements in solution (IUPAC Technical Report), *Pure and Applied Chemistry*. 83 (2011) 2213–2228. <https://doi.org/10.1351/PAC-REP-10-09-31>.
- [52] E. Wexselblatt, E. Yavin, D. Gibson, Cellular interactions of platinum drugs, *Inorganica Chimica Acta*. 393 (2012) 75–83. <https://doi.org/10.1016/j.ica.2012.07.013>.
- [53] J.D. White, M.M. Haley, V.J. DeRose, Multifunctional Pt(II) Reagents: Covalent Modifications of Pt Complexes Enable Diverse Structural Variation and In-Cell Detection, *Acc. Chem. Res.* 49 (2016) 56–66. <https://doi.org/10.1021/acs.accounts.5b00322>.
- [54] E.C. Sutton, C.E. McDevitt, M.V. Yglesias, R.M. Cunningham, V.J. DeRose, Tracking the cellular targets of platinum anticancer drugs: Current tools and emergent methods, *Inorganica Chimica Acta*. 498 (2019) 118984. <https://doi.org/10.1016/j.ica.2019.118984>.

